Research

New Phytologist

Uncoupling of stomatal conductance and photosynthesis at high temperatures: mechanistic insights from online stable isotope techniques

Haoyu Diao[1]*, Lucas A. Cernusak[2], Matthias Saurer[1], Arthur Gessler[1,3], Rolf T. W. Siegwolf[1] and Marco M. Lehmann[1]*

[1]Swiss Federal Institute for Forest, Snow and Landscape Research WSL, Birmensdorf, 8903, Switzerland; [2]College of Science and Engineering, James Cook University, Cairns, Qld, 4879, Australia; [3]Institute of Terrestrial Ecosystems, ETH Zurich, Zurich, 8092, Switzerland

Authors for correspondence:
Haoyu Diao
Email: haoyu.diao@wsl.ch

Marco M. Lehmann
Email: marco.lehmann@wsl.ch

Received: *20 November 2023*
Accepted: *12 January 2024*

New Phytologist (2024) **241:** 2366–2378
doi: 10.1111/nph.19558

Key words: carbon isotopes, leaf gas exchange, mesophyll conductance, oxygen isotopes, vapour pressure deficit.

Summary

- The strong covariation of temperature and vapour pressure deficit (VPD) in nature limits our understanding of the direct effects of temperature on leaf gas exchange. Stable isotopes in CO_2 and H_2O vapour provide mechanistic insight into physiological and biochemical processes during leaf gas exchange.
- We conducted combined leaf gas exchange and online isotope discrimination measurements on four common European tree species across a leaf temperature range of 5–40°C, while maintaining a constant leaf-to-air VPD (0.8 kPa) without soil water limitation.
- Above the optimum temperature for photosynthesis (30°C) under the controlled environmental conditions, stomatal conductance (g_s) and net photosynthesis rate (A_n) decoupled across all tested species, with g_s increasing but A_n decreasing. During this decoupling, mesophyll conductance (cell wall, plasma membrane and chloroplast membrane conductance) consistently and significantly decreased among species; however, this reduction did not lead to reductions in CO_2 concentration at the chloroplast surface and stroma.
- We question the conventional understanding that diffusional limitations of CO_2 contribute to the reduction in photosynthesis at high temperatures. We suggest that stomata and mesophyll membranes could work strategically to facilitate transpiration cooling and CO_2 supply, thus alleviating heat stress on leaf photosynthetic function, albeit at the cost of reduced water-use efficiency.

Introduction

A rise in vapour pressure deficit (VPD) has become evident in recent decades, due to a significant increase in surface temperature, while surface relative humidity (RH) has declined at the global scale (Vicente-Serrano *et al.*, 2018; IPCC, 2021). Plants sense variations in VPD, defined as the difference between the saturation and actual water vapour pressure, through the leaf-to-air vapour pressure difference (LAVPD). LAVPD is derived from leaf temperature (T_{leaf}), which influences the saturation vapour pressure inside the leaf. An increasing number of studies have shown the significant role of temperature and LAVPD increases in climate-change-induced tree mortality and growth decline (Novick *et al.*, 2016; Grossiord *et al.*, 2020; Trotsiuk *et al.*, 2021; McDowell *et al.*, 2022). Still, uncertainty and potential heterogeneity in the future VPD trend exist, as there are reports of increasing, instead of decreasing, trends in surface RH with warming at regional scales (Singh *et al.*, 2008; Eludoyin *et al.*, 2014; Khan *et al.*, 2022). More importantly, the interconnected nature of temperature and LAVPD complicates efforts to better understand and model plant responses to a changing environment, which highlights the need to disentangle the effects of temperature and LAVPD (Smith *et al.*, 2020; Schönbeck *et al.*, 2022).

The exchange of carbon (C) and water (H_2O) in leaves is a key component of plant–environment interactions. The response of this leaf gas exchange to temperature has been examined intensively in previous studies, as temperature is a critical driver of numerous physiological and biochemical processes (von Caemmerer & Farquhar, 1981; Lawson *et al.*, 2011; Crous *et al.*, 2022). It is believed that, under a constant VPD, net photosynthesis rate (A_n) and transpiration rate (E) or stomatal conductance (g_s) typically respond in parallel to changes from low to high T_{leaf}, showing an increasing and a decreasing trend before and after the optimum temperature for photosynthesis, respectively (Wong *et al.*, 1979; Hamerlynck & Knapp, 1996; Lawson *et al.*, 2011; Duursma *et al.*, 2014). However, some studies have provided experimental and observational evidence of a

*These authors contributed equally to this work.

possible decoupling of A_n and E or g_s (Schulze *et al.*, 1973; Ameye *et al.*, 2012; von Caemmerer & Evans, 2015; Drake *et al.*, 2018; De Kauwe *et al.*, 2019; Krich *et al.*, 2022; Feng *et al.*, 2023). Here, the decoupling specifically refers to a decrease in A_n and an increase in g_s with increasing temperature. Such a decoupling indicates a reduced water-use efficiency (WUE, defined as A_n/E) under heat stress. However, these studies were not able to isolate the direct temperature effect by measuring at a constant LAVPD, mostly because of technical difficulties regarding humidity control across large temperature ranges. Conversely, leaf-scale gas exchange measurements have been made under constant LAVPD conditions (Hall *et al.*, 1975; Hall & Kaufmann, 1975; Osonubi & Davies, 1980; Aphalo & Jarvis, 1991; Fredeen & Sage, 1999; Mott & Peak, 2010), but only the study of Urban *et al.* (2017) observed the decoupling when T_{leaf} increased from 30 to 40°C at a LAVPD of 1 kPa for both *Populus deltoides* × *nigra* (poplar) and *Pinus taeda* (loblolly pine). Our understanding of the mechanisms of temperature effects on leaf gas exchange clearly remains limited, especially when plants are exposed to temperatures outside their optimal range. Such conditions are becoming increasingly relevant, as hot and cold temperature extremes are becoming more frequent and severe in many parts of the world (Perkins *et al.*, 2012; Seneviratne *et al.*, 2014; Frank *et al.*, 2015). Moreover, coupling of the temperature responses of A_n and g_s has been a key assumption of many leaf-level stomatal models (Farquhar & Wong, 1984; Ball *et al.*, 1987; Leuning *et al.*, 1995; Damour *et al.*, 2010). A better understanding of the direct influence of temperature on leaf gas exchange, including when and how A_n and g_s become decoupled, would contribute to more accurate predictions of the consequences of climate change.

Stable isotopes in carbon dioxide (CO_2) and H_2O have been used to improve our understanding of various processes of leaf gas exchange, because of the isotopic fractionation that co-occurs during these processes (Farquhar *et al.*, 1982; Cernusak *et al.*, 2016; Siegwolf *et al.*, 2023). The combined instrumentation of infrared gas analysers and isotope laser spectrometers has facilitated measurements of C and oxygen (O) isotopic composition ($\delta^{13}C$ and $\delta^{18}O$) in CO_2 and H_2O entering and leaving a leaf gas exchange chamber in real-time under controlled conditions (Evans *et al.*, 1986; Barbour, 2017). This allows the tracing of CO_2 and H_2O travelling along the pathway of chloroplast, cell wall, stoma and leaf boundary layer, providing additional information on physiological processes occurring at the leaf level (Kodama *et al.*, 2011; Sonawane & Cousins, 2019). Photosynthetic ^{13}C discrimination ($\Delta^{13}C$), which is modulated by the intercellular (c_i) and chloroplastic CO_2 mole fraction (c_c), reflects the interplay between A_n and g_s during leaf gas exchange (Wingate *et al.*, 2007). The ^{18}O fractionation in the CO_2 molecule occurs at the sites of carbonic anhydrase catalysis (c_{ca}), where the equilibration of ^{18}O in CO_2 and H_2O takes place. The chloroplast surface is thought to be the major site of the equilibration. The equilibrated CO_2 can diffuse back and mix with the CO_2 from the atmosphere that diffused into the intercellular air space (Gillon & Yakir, 2000). Assuming that the $\delta^{18}O$ of H_2O at the chloroplast surface is very close to that at the evaporative sites, the $\delta^{18}O$ in CO_2 in the intercellular air spaces ($\delta^{18}O_i$) can be used to infer the ^{18}O enrichment of leaf water at the sites of evaporation. According to the Craig–Gordon model (Craig & Gordon, 1965; Farquhar *et al.*, 2007), this is largely determined by the ratio of leaf external to internal water vapour pressure (equal to RH if T_{leaf} is assumed to be close to ambient air temperature).

The isotopic approach can also be applied to rapidly estimate mesophyll conductance to CO_2 (g_m; Kodama *et al.*, 2011; Barbour *et al.*, 2016; Holloway-Phillips *et al.*, 2019; Sonawane & Cousins, 2019), which has been recognized as an important limiting factor for photosynthesis. Total mesophyll conductance (g_{m13}; definitions of symbols can be found in Table 1) can be estimated from $\Delta^{13}C$ measurements, while O isotope fractionation measurements can provide information on cell wall and plasma membrane conductance (g_{m18}; Gillon & Yakir, 2000). The difference between the two is therefore the chloroplast membrane conductance (g_{cm}). Studies have shown either a monotonic increase or peaked response of g_m to increasing temperature (Warren & Dreyer, 2006; Yamori *et al.*, 2006; Evans & von Caemmerer, 2013; Walker *et al.*, 2013; von Caemmerer & Evans, 2015; Shrestha *et al.*, 2019). von Caemmerer & Evans (2015) used a simplified model to describe the temperature dependence of g_m, but they were not able to explain the observed g_m decline at high temperatures. Flexas & Diaz-Espejo (2015) proposed the explanation of a progressive reduction in the chloroplast surface area facing the intercellular air space as a result of increased LAVPD with increasing temperature. Again, because the measurements were not conducted at

Table 1 Definitions of symbols used repeatedly in the main text.

Symbol	Definition
A_n	Net photosynthesis rate
c_a	CO_2 mole fraction in the atmosphere
c_c	CO_2 mole fraction in the chloroplast
c_{ca}	CO_2 mole fraction at the sites of carbonic anhydrase activity
c_i	CO_2 mole fraction in the leaf intercellular air space
$\delta^{18}O_i$	$\delta^{18}O$ of CO_2 in the intercellular air spaces
$\Delta^{13}C$	Net/apparent discrimination against ^{13}C during net CO_2 uptake by photosynthesis
$\Delta^{13}C_{obs}$	Observed net/apparent discrimination against $^{13}CO_2$ during photosynthesis
E	Transpiration rate
g_{cm}	Chloroplast membrane conductance to CO_2
g_m	Mesophyll conductance to CO_2
g_{m13}	Mesophyll conductance to CO_2 estimated from ^{13}C measurements, representing the total mesophyll conductance
g_{m18}	Mesophyll conductance to CO_2 estimated from ^{18}O measurements, representing the cell wall and plasma membrane conductance
g_s	Stomatal conductance to H_2O
LAVPD	Leaf-to-air vapour pressure difference
RH	Relative humidity
T_{cuv}	Cuvette temperature
T_{leaf}	Leaf temperature
WUE	Water-use efficiency

Symbols that appear only alongside their definition in the text are not included here.

constant LAVPD in these studies, the direct temperature response of g_m has remained unclear.

Here, we aimed to: (1) assess the direct temperature responses of leaf gas exchange, isotope fractionation and g_m under stable, nonlimiting soil water supply and stable, low LAVPD conditions; and (2) utilize stable isotope measurements, complementing gas exchange measurements, to gain better mechanistic insights into the temperature response of gas diffusion processes within the leaf. To pursue these objectives, we carried out combined gas exchange and online isotope fractionation measurements on four common European tree species: *Fagus sylvatica* L., *Picea abies* (L.) *H. Karst.*, *Quercus petraea* (*Matt.*) *Liebl.* and *Tilia cordata Mill.* (Supporting Information Fig. S1). We used a novel instrumental set-up (Fig. S2), which ensured that the measurements were performed over a large and physiologically relevant temperature range (5–40°C) under a low and constant LAVPD (0.8 kPa).

Materials and Methods

Plant material

Five 2-yr-old saplings of *Fagus sylvatica* L., *Picea abies* (L.) *H. Karst.*, *Quercus petraea* (*Matt.*) *Liebl.* and *Tilia cordata Mill.* were transplanted into 4-l pots with soil mixed with commercial slow-release NPK fertilizer (Osmocote Exact Standard 3–4 M; ICL, Suffolk, UK). The plants were transferred to a climate chamber (Bitzer 6HE-35Y; Kälte 3000 AG, Landquart, Switzerland) to induce leaf flushing. The environmental conditions were air temperature of 25°C, RH of 60% and light intensity of 110 µmol m^{-2} s^{-1} during a photoperiod of 18 h, and air temperature of 15°C and RH of 50% during night time. One month later, the plants were transferred to a glasshouse and grew under natural light conditions. The plants were watered every 2 d, such that trays beneath the pots always contained some liquid water. During the period when the plants were in the glasshouse (from 14 April to 20 July 2022), the average air temperature was 22.8°C and the average RH was 54.1%.

Gas exchange system and isotopic analysers

A schematic illustration of the pneumatic flows of the gas exchange system and isotopic analysers is shown in Fig. S2. The leaf gas exchange system included a portable photosynthesis control unit (GFS-3000), a leaf cuvette (3010-GWK1), a light-emitting diode (LED) light source (RGBW-L084) and a bypass humidity control system (NFRB0101, all components from Heinz Walz GmbH, Effeltrich, Germany).

The leaf cuvette was temperature-controlled and had a volume of 320 ml, which was large enough to accommodate one entire leaf or a foliated branch. An adjustable transversal fan inside the cuvette was used to thoroughly mix the air, minimizing the leaf boundary layer resistance and ensuring a homogeneous T_{cuv}, humidity and CO_2 concentration (c_a) distribution. T_{leaf} measured using a thermocouple (3010-CA/TCL; Heinz Walz GmbH) and photosynthetically active radiation (PAR) measured using a mini quantum sensor (LS-C; Heinz Walz GmbH) were recorded continuously.

The bypass humidity control system was designed to optimize the humidity control processes of the GFS-3000, to keep the preselected humidity in the cuvette constant by removing the transpired H_2O vapour. The signal of the H_2O vapour mole fraction measured by the GFS-3000 was used to control the bypass pump via a proportional–integral–derivative controller. Cuvette gas was pumped at a rate proportional to E through a Nafion drier (PD-200T-24MSS; Perma Pure LLC, Burnaby, BC, Canada), and flow rates were measured with an integrated mass flow meter (Heinz Walz GmbH). The H_2O vapour mole fraction of the dried gas was determined using a dew point mirror (TS-2; Heinz Walz GmbH) before it was reintroduced into the cuvette.

All metal surfaces in the dew point mirror housings and in the leaf cuvette were nickel-plated to minimize adhesion of H_2O vapour and thereby memory effects. The whole gas exchange system was positioned inside a climate chamber with a volume of *c.* 2.2 m^3 (Conviron PGR15; Controlled Environments Ltd, Winnipeg, MB, Canada). Thus, the temperature of the tubing and peripheral components was kept at the same level as the leaf inside the cuvette, to avoid potential condensation and to keep the whole plant at similar conditions regarding air temperature, humidity and PAR.

The gas exchange system was coupled to a CO_2 isotope ratio infrared spectrometer (IRIS; Delta Ray, Thermo Fisher Scientific Inc., Bremen, Germany) and a H_2O cavity ring-down spectrometer (CRDS; L2120-i, Picarro Inc., Santa Clara, CA, USA). With an interposed multi-port valve (VICI; Valco Instruments Co. Inc., Houston, TX, USA), the air streams entering (reference) or leaving (sample) the leaf cuvette were selected alternately for analysis. The gas exchange system and the VICI valve were connected via an open split to prevent pressure surges caused by valve switching. The open split comprised a 1.6 mm diameter stainless steel tube inserted into a 3.1 mm diameter stainless steel tube via a three-way connector (SS-200-3; Swagelock, Solon, OH, USA). A 20-cm tube connected to the third opening vented excess gas flow from the gas exchange system. The outlet flow rate of the gas exchange system was much higher than the total inflow rate of the two isotope spectrometers, preventing ambient air intrusion at the open splits. The VICI valve and open splits were placed inside the climate chamber. The tube connecting the VICI valve to the isotope spectrometers was heated to 65°C using a heating band (HTS System AG, Hünenberg, Switzerland). The inflow gas for the CO_2 isotopic measurements was dried using magnesium perchlorate [$Mg(ClO_4)_2$] before entering the IRIS.

Instrument calibrations

CO_2 and H_2O concentration zero-point and span calibrations were carried out weekly for the gas exchange system. The zero-point calibrations were carried out by measuring CO_2-free and dry air generated using fresh soda lime and silica gel, respectively. The span calibrations were carried out by measuring two gases with defined CO_2 concentrations of 350 and 1350 µmol mol^{-1} and gases with defined H_2O vapour mole fractions (8.71 and 25.01 mmol mol^{-1}) generated by a dew point generator (Li-610; Li-Cor, Lincoln, NE, USA).

Built-in calibration programs of the CO_2 isotope analyser were conducted weekly for both the CO_2 concentration dependency of the isotope ratio and the span of the isotope ratio and CO_2 concentration. For the concentration dependence correction, a pure CO_2 reference gas with known isotope ratios (Isotope Ref. Gas1: $\delta^{13}C$ of −9‰ Vienna Pee Dee Belemnite (VPDB) and $\delta^{18}O$ of −13.2‰ VPDB-CO_2) was diluted with CO_2-free synthetic air to various concentrations between 200 and 3500 µmol mol^{-1} and isotope ratios measured. A polynomial function was then fitted to normalize the measured values to true values. Following the concentration dependence correction, the span calibrations were performed sequentially on two different pure CO_2 reference gases with known isotope ratios (Isotope Ref. Gas1 and Isotope Ref. Gas2: $\delta^{13}C$ of −25.5‰ VPDB and $\delta^{18}O$ of −24.4‰ VPDB-CO_2; Thermo Fisher Scientific Inc.), which were diluted to a CO_2 concentration of 450 µmol mol^{-1}, as well as two different reference gases with known CO_2 concentrations (362.1 and 1154 µmol mol^{-1}). A linear function was then fitted to normalize the measured values to true values. Note that the CO_2 isotope analyser reported $\delta^{18}O$ of CO_2 against VPDB-CO_2, which was subsequently converted to the Vienna Standard Mean Ocean Water (VSMOW) scale for further data analyses (Mook, 2000): $\delta^{18}O_{VSMOW} = 1.04143 \times \delta^{18}O_{VPDB\text{-}CO2} + 41.43$.

The H_2O isotope analyser was calibrated daily using a standard delivery module (A0101; Picarro Inc.) coupled to a vaporization module (V1102-I; Picarro Inc.). For the calibration, two different H_2O samples with known $\delta^{18}O$ values (−9.84‰ and −26.82‰) were injected at a defined flow speed by the standard delivery module to the vaporization module and vaporized at 140°C. The H_2O vapour was subsequently introduced into the analyser with dry air as a carrier gas. A linear function was fitted to the measured values against the true values; the calibration coefficients (slope and intercept) were averaged and then used to calibrate the raw data from the whole measurement period.

Measurement protocol

One day before the measurements, plants of a species were transferred from the glasshouse to the climate chamber. During the measurements, one foliated branch (for *F. sylvatica* and *P. abies*) or one entire leaf (for *Q. petraea* and *T. cordata*) was placed in the cuvette. T_{cuv} was increased from 5 to 40°C in steps of *c.* 5°C. For each T_{cuv} step, the target LAVPD was 0.8 kPa, PAR was set to 800 µmol m^{-2} s^{-1} (light saturation), c_a was kept constant at 400 µmol mol^{-1}, and the flow rate through the cuvette was set to 730 µmol s^{-1}. In addition, air temperature and RH in the climate chamber were set to match the values in the leaf cuvette. During the dark phase (night-time, from 20:00 h to 06:00 h), the temperature in the climate chamber was reduced by 5°C from the highest temperature value reached during the day, while maintaining the VPD at the same level as during the day. As soon the gas exchange rates were at steady state, the gas exchange data were recorded, and the reference gas and the sample gas were selected sequentially to measure and record their isotope ratio. Scanned leaf area was taken to relate the calculated leaf gas exchange values to 1 m^2 leaf area; for *P. abies*, the scanned needle area was doubled to account for the total surface (Kupper *et al.*, 2006).

Calculations

As a supplement to Table 1, additional symbols used in the calculations, as well as their definitions, are listed in Table S1. The gas exchange-related parameters (i.e. A_n, c_i, E, g_s) were obtained directly from the Walz photosynthesis system. These parameters were calculated according to the approach of von Caemmerer & Farquhar (1981).

In the following calculations, $\delta^{13}C$ of CO_2 was scaled to VPDB and $\delta^{18}O$ of CO_2 was scaled to VSMOW. The online C or O isotope discrimination of the leaf (Δ_{obs}) was calculated from corresponding measurements of the $\delta^{13}C$ or $\delta^{18}O$ of the CO_2 entering and leaving the cuvette (Evans *et al.*, 1986):

$$\Delta_{obs} = \frac{\xi(\delta_a - \delta_{in})}{1 + \delta_a - \xi(\delta_a - \delta_{in})} \quad \text{Eqn 1}$$

where δ_a is the $\delta^{13}C$ or $\delta^{18}O$ of CO_2 leaving the cuvette and δ_{in} is that of CO_2 entering the cuvette. The term ξ is defined as:

$$\xi = \frac{c_{in}}{c_{in} - c_a} \quad \text{Eqn 2}$$

where c_{in} and c_a are the CO_2 concentrations in air entering the cuvette and leaving the cuvette, respectively (µmol mol^{-1}). The values used in Eqn 2 were CO_2 concentrations in dry air, obtained by the equation $c_{dry} = c_{wet}/(1 - w)$, where w is the H_2O vapour mole fraction in the air (mol mol^{-1}), because no flow rate correction for the influence of different H_2O vapour concentrations entering and leaving the cuvette was applied in deriving Eqn 1.

Δ_{obs} for C isotopes can then be compared with modelled C isotope discrimination (Δ_i), applying the assumption that c_c equals c_i to allow the estimation of g_{m13}. The most recent iteration of the definition of Δ_i, presented by Busch *et al.* (2020), is:

$$\Delta_i = \frac{1}{1-t}\left[a_b\frac{c_a - c_s}{c_a} + a_s\frac{c_s - c_i}{c_a}\right] + \frac{1+t}{1-t}$$
$$\left[b\frac{c_i}{c_a} - \frac{\alpha_b}{\alpha_e\alpha_R}e'\frac{R_{day}}{A_n}\frac{c_i}{c_a} - \frac{\alpha_b}{\alpha_f\alpha_R}\frac{\Gamma^*}{c_a}(f - wh)\right] \quad \text{Eqn 3}$$

Eqn 3 incorporates the original formulation by Farquhar *et al.* (1982) and the ternary correction introduced by Farquhar & Cernusak (2012). Dark respiration measurements were performed to estimate the rate of day respiration (R_{day}). The measurements were conducted at T_{cuv} of 10, 20, 30 and 40°C under dark conditions for each species. c_a was kept constant at 400 µmol mol^{-1}, and the flow rate was set to 730 µmol s^{-1}. For each species, the dark respiration rate (R_{dark}) at T_{leaf} was estimated by fitting an exponential relationship: $R_{dark} = a_r + \exp$

($b_r \times T_{leaf}$), where a_r and b_r are coefficients of this function. R_{day} was then estimated by assuming that the ratio of R_{day} to the rate of R_{dark} is 0.5 (Adnew *et al.*, 2020). In Eqn 3, t is the ternary correction term, c_s is the CO_2 mole fraction at the leaf surface, and Γ^* is the CO_2 compensation point in the absence of day respiration. The calculations of t, c_s and Γ^* can be found in Methods S1.

In Eqn 3, a_b is the $^{13}C/^{12}C$ fractionation for CO_2 diffusion across the boundary layer (2.9‰), and a_s is that for CO_2 diffusion through the stomata (4.4‰). The term b is the $^{13}C/^{12}C$ fractionation associated with carboxylation, mainly by Rubisco in C_3 plants (30‰), and f is the $^{13}C/^{12}C$ fractionation during photorespiration (11‰). $e' = e + e^*$, where e is the $^{13}C/^{12}C$ fractionation during day respiration (−3‰), and e^* is $(\delta_{a(obs)} - \Delta_{obs}) - (\delta_{a(growth)} - \Delta_{growth})$, where $\delta_{a(obs)}$ is the $\delta^{13}C$ of CO_2 in the cuvette during the online measurements, $\delta_{a(growth)}$ is the $\delta^{13}C$ of CO_2 in the air in the growth environment, and Δ_{growth} is the discrimination under growth conditions. This accounts for the difference between the $\delta^{13}C$ of assimilates produced during photosynthesis and that of the likely substrate for respiration (Wingate *et al.*, 2007). In the calculations, e^* was assumed to equal zero, because each leaf spent several hours in the gas exchange cuvette, during which the respiratory pool of assimilates was turning over. Turnover was therefore assumed to be sufficiently effective in replacing the active respiratory pool with assimilates formed while the leaf was in the cuvette. The terms α_b, α_e and α_f in Eqn 3 are defined as $1 + b$, $1 + e$ and $1 + f$, respectively. For calculations of the α terms, the corresponding $^{13}C/^{12}C$ fractionation factors had to be divided by 1000. The term α_R, introduced by Busch *et al.* (2020), is defined as $1 + (R_{day}/A_n)(e/\alpha_e)$. The term h, introduced by Busch *et al.* (2020), is the fractionation that could occur with export of triose phosphates from the Calvin cycle. Its value is unknown; therefore, it is assumed to be 0‰, in absence of a better estimate. The term w was defined by Busch *et al.* (2020) as $(6c_c + 9\Gamma^*)/(5c_c + 10\Gamma^*)$, but as it is multiplied by h, the combined term wh becomes zero.

g_{m13} was calculated as:

$$g_{m13} = \frac{1+t}{1-t}\left(\frac{b - a_m - \frac{\alpha_b}{\alpha_e \alpha_R} e' \frac{R_{day}}{A_n}}{\Delta_i - \Delta_{obs}}\right)\frac{A_n}{c_a} \quad \text{Eqn 4}$$

where a_m is the $^{13}C/^{12}C$ fractionation for CO_2 dissolution and diffusion from the intercellular air spaces to the sites of carboxylation in the chloroplasts (1.8‰).

c_c was then calculated as:

$$c_c = c_i - \frac{A_n}{g_{m13}} \quad \text{Eqn 5}$$

The $\delta^{18}O$ of CO_2 taken up by photosynthesis was calculated based on the Δ_{obs} of $^{18}O/^{16}O$ (Eqn 1). Note that the enrichment of ^{18}O in CO_2 as it passes through the cuvette does not come from a discrimination within the photosynthetic process, but rather from the exchange of O atoms with the enriched leaf water. Nonetheless, by writing the equations somewhat analogously to those for ^{13}C, the apparent $\delta^{18}O$ of assimilated CO_2 (δ_A) could be calculated as:

$$\delta_A = \frac{\delta_a - \Delta_{obs}}{1000 + \Delta_{obs}} \quad \text{Eqn 6}$$

The $\delta^{18}O$ of CO_2 in the intercellular air spaces, with the ternary correction (δ_i), was calculated as follows (Cernusak *et al.*, 2004; Farquhar & Cernusak, 2012):

$$\delta_i = \frac{\delta_A\left(1 - \frac{c_a}{c_i}\right)\alpha_{ac} + \frac{c_a}{c_i}(\delta_a - \bar{a}) + \bar{a} + t\left[\delta_A\left(\frac{c_a}{c_i} + 1\right) - \delta_a \frac{c_a}{c_i}\right]}{1 + t} \quad \text{Eqn 7}$$

where the $\bar{a}$ is the weighted fractionation during diffusion of CO_2 into the intercellular air spaces for ^{18}O. The calculations for $\bar{a}$ can be found in Methods S1.

The $\delta^{18}O$ of CO_2 at the site of carbonic anhydrase activity (δ_{ce}), where equilibration of ^{18}O in CO_2 and H_2O takes place, was then calculated from the measurements of the $\delta^{18}O$ of transpired H_2O:

$$\delta_{ce} = \delta_e(1 + \varepsilon_w) + \varepsilon_w \quad \text{Eqn 8}$$

where δ_e is the $\delta^{18}O$ of the liquid H_2O at the evaporative site in the leaf, and ε_w is the equilibrium fractionation between H_2O and CO_2. The calculations for δ_e and ε_w can be found in Methods S1.

c_{ca} was calculated according to Barbour *et al.* (2016):

$$c_{ca} = c_i\left(\frac{\delta_i - \bar{a} - \alpha_{ac}\delta_A}{\delta_{ce} - \bar{a} - \alpha_{ac}\delta_A}\right) \quad \text{Eqn 9}$$

where α_{ac} is defined as $1 + \bar{a}$.

Finally, g_{m18} was calculated as:

$$g_{m18} = \frac{A_n}{c_i - c_{ca}} \quad \text{Eqn 10}$$

Statistical analysis

All statistical analyses were conducted using R software v.4.3.1 (R Core Team, 2023). To analyse the isotopic parameters, a filter of $\xi < 30$ (see Table S2) was applied to exclude measurements with a small difference in CO_2 mole fractions between the reference and sample gas, which represents low confidence in the isotopic discrimination estimates. For both g_{m13} and g_{m18}, values < -0.1 mol m^{-2} s^{-1} and > 0.5 mol m^{-2} s^{-1} were additionally excluded (5.3% of all g_{m13} values and 16% of all g_{m18} values). These cases could have been caused by measurement inaccuracy and/or propagation and by an accumulation of errors during the calculations. With a local polynomial regression fitting, a smoothed trend was obtained for each species separately and for all species together, to show the individual and general patterns of responses of gas exchange, isotopic discrimination, and g_m to T_{leaf}. The responses of these

variables to T_{leaf} were further analysed using linear mixed models with the IMERTEST package in R (Kuznetsova *et al.*, 2017), with T_{leaf} as a fixed effect and species as a random effect. To test whether the temperature responses were linear, generalized additive models (GAM) were fitted using an iteratively reweighted least squares method. This was performed using the GAM package in R (Hastie, 2023). The relationship was considered linear if the nonlinear terms in the fitted GAM were not significantly different from zero.

Results

LAVPD remained relatively constant during all measurements, with a mean value (±1 SD) of 0.82 (±0.11) kPa at different cuvette temperature (T_{cuv}) steps, indicating good humidity control of the gas exchange system (Fig. 1). RH increased with the increase in T_{cuv}, following the theoretical relationship between RH and temperature at a constant VPD. The linear regression of T_{leaf} against T_{cuv} ($R^2 = 1.00$, $P < 0.001$) had a slope of 0.992, and T_{leaf} was slightly higher (by 0.41 ± 0.22°C) compared with T_{cuv} over the tested temperature range (Fig. S3a). The difference between T_{leaf} and T_{cuv} decreased by *c.* 0.5°C with an increase in E from 0 to 3 mmol H_2O m^{-2} s^{-1} in three out of the four species ($P < 0.001$), with the exception being *P. abies* ($P = 0.054$; Fig. S3b).

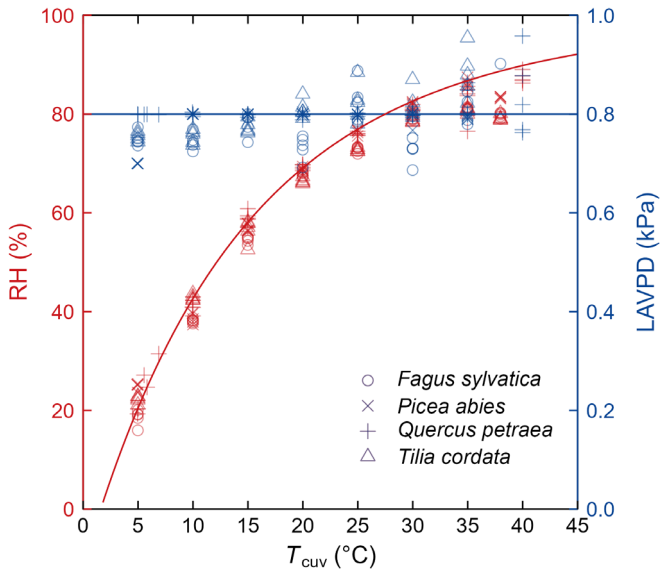

Fig. 1 Variations in relative humidity (RH) and leaf-to-air vapour pressure difference (LAVPD) with increasing cuvette temperature (T_{cuv}). RH and T_{cuv} were measured using capacitive humidity sensors and Pt100 temperature sensors in the cuvette. The blue line indicates LAVPD = 0.8 kPa, which was the target LAVPD across the different temperature steps in the experiments. The red line is the theoretical relationship between RH and T when VPD = 0.8 kPa, which is derived from the temperature dependence of saturation vapour pressure calculated with the formula of Goff–Gratch (Goff & Gratch, 1946). Symbols indicate different tree species ($n = 5$, per step of *c.* 5°C).

Responses of leaf gas exchange to temperature

Responses of gas exchange parameters (A_n, E, g_s and c_i/c_a) to T_{leaf} were consistent among the four species overall (Fig. 2). In general, A_n first increased, peaking at *c.* 30°C, then decreased with a further increase in T_{leaf} (Fig. 2a; $F = 108.63$, $P < 0.001$). At the highest temperature tested (40°C), A_n reduced to a level similar to that *c.* 15–20°C. By contrast, E showed a curvilinear increase in response to increasing T_{leaf} for all species (Fig. 2b; $F = 229.54$, $P < 0.001$). As a result of the divergent temperature responses of A_n and E, WUE increased with increasing T_{leaf} until *c.* 25°C and then decreased dramatically to nearly 2 mmol CO_2 mol^{-1} H_2O with further increases in T_{leaf} (Fig. S4; $F = 62.58$, $P < 0.001$). Similar to E, g_s increased with increasing T_{leaf} (Fig. 2c; $F = 183.54$, $P < 0.001$); however, a GAM showed that the increasing trend in g_s with T_{leaf} was described adequately using a linear relationship, as the smooth term in the fitted model was not statistically significant ($P = 0.06$). c_i/c_a initially decreased with increasing T_{leaf}, reaching a minimum *c.* 20–25°C, then increased with a further increase in T_{leaf} (Fig. 2d; $F = 40.38$, $P < 0.001$). c_i/c_a was higher at 40°C than at 5°C (Fig. 2d). Note that for *F. sylvatica*, g_s and E were relatively less responsive to changes in T_{leaf} at the low end of the temperature range (5–20°C; Fig. 2b,c) compared with the other species. As a result, the lowest value of c_i/c_a and the highest value of WUE occurred at *c.* 15–20°C for *F. sylvatica*, but *c.* 25–30°C for the other species (Figs 2d, S4).

Carbon and oxygen isotope discrimination during leaf CO_2 exchange

We found an overall significant response of observed ^{13}C photosynthetic discrimination ($\Delta^{13}C_{obs}$) to T_{leaf} for all species (Fig. 3a; $F = 47.16$, $P < 0.001$). With the increase in T_{leaf}, $\Delta^{13}C_{obs}$ decreased precipitously, from 28.2‰ to 19.5‰ between 5 and 15°C (Fig. 3a). Above *c.* 15°C, $\Delta^{13}C_{obs}$ varied subtly with an average of 18.7‰ (Fig. 3a). Contrary to the positive temperature responses of E and g_s (Fig. 2b,c), $\delta^{18}O_i$ showed a curvilinear decrease with increasing T_{leaf} ($F = 352.3$, $P < 0.001$), with values averaged across all species diminishing from 61‰ to 39‰.

Responses of mesophyll conductance and chloroplastic CO_2 concentration to temperature

Across species, g_{m13}, g_{m18} and g_{cm} had significant quadratic responses to T_{leaf} (Fig. 4; g_{m13}: $F = 13.00$, $P < 0.001$; g_{m18}: $F = 22.09$, $P < 0.001$; and g_{cm}: $F = 14.13$, $P < 0.001$), showing first an increase and then a decrease with increasing T_{leaf}. While g_{m13} peaked between 20 and 25°C (Fig. 4a), g_{m18} peaked at 20°C (Fig. 4b). As a result, g_{cm} peaked at 25°C (Fig. 4c). Across all species and measured temperatures, mean values (±1 SD) were 0.11 (±0.08) for g_{m13}, 0.12 (±0.10) mol m^{-2} s^{-1} for g_{m18} and 0.25 (±0.28) mol m^{-2} s^{-1} for g_{cm}.

Both c_c/c_a and c_{ca}/c_a showed significant responses to T_{leaf} ($F = 20.61$, $P < 0.001$ and $F = 38.54$, $P < 0.001$, respectively; Fig. 5). c_c/c_a decreased dramatically from 5 to 15°C but did not

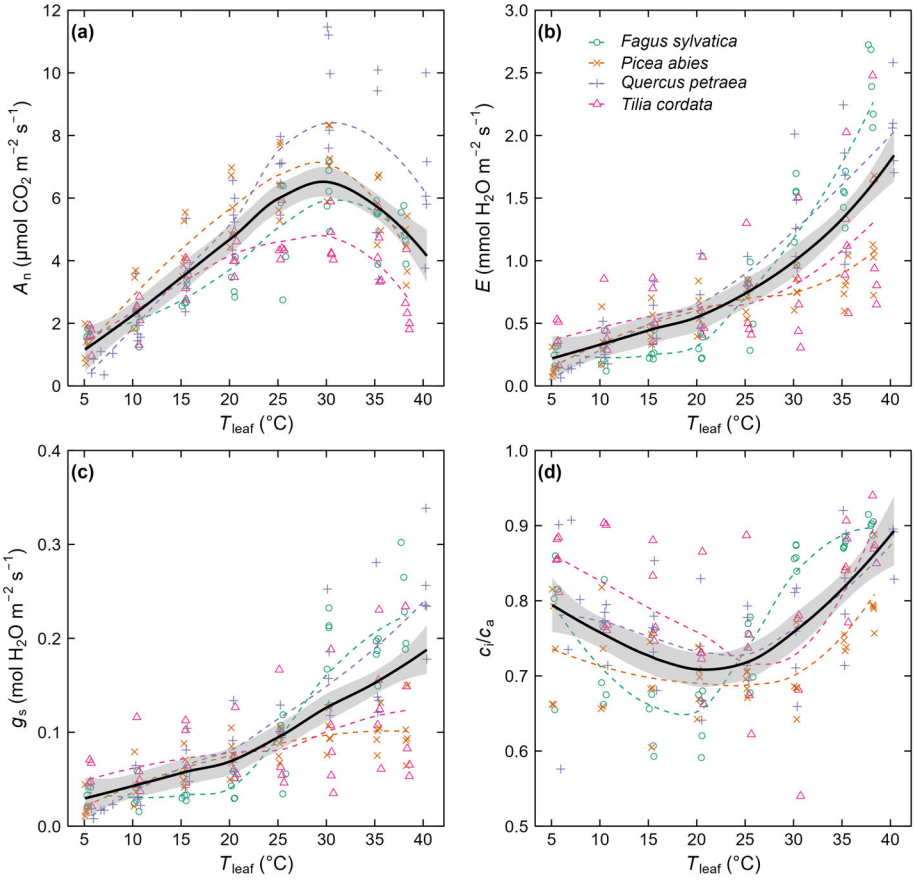

Fig. 2 Gas exchange responses to increasing leaf temperature (T_{leaf}) in four temperate tree species. We show net photosynthesis rate, A_n (a); transpiration, E (b); stomatal conductance, g_s (c); and the ratio of intercellular to ambient CO_2 mole fraction, c_i/c_a (d). Each dashed line represents the smoothed trend for one species. The solid line and the grey band represent the smoothed trend averaged across all species and its SE, respectively. Different symbols and colours indicate different tree species ($n = 5$, per step of *c*. 5°C).

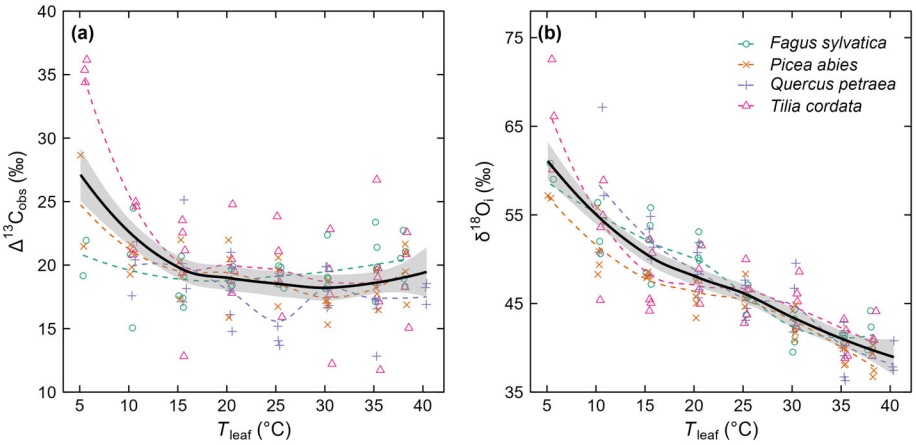

Fig. 3 Responses of online discrimination against $^{13}CO_2$ ($\Delta^{13}C_{obs}$; a) and of $\delta^{18}O$ of CO_2 in the intercellular air spaces ($\delta^{18}O_i$; b) to leaf temperature (T_{leaf}) in four temperate tree species. Each dashed line represents the smoothed trend for one species. The solid line and the grey band represent the smoothed trend averaged across all species and its SE, respectively. Different symbols and colours indicate different tree species ($n = 5$, per step of *c*. 5°C).

decrease further with increasing T_{leaf}. It was rather invariant between 20 and 40°C; however, it showed a slight increase above 30°C (Fig. 5a). c_{ca}/c_a showed a decreasing trend from 5 to 30°C, then increased dramatically with further increases in T_{leaf} (Fig. 5b).

Discussion

Maintaining constant low LAVPD at high temperatures is challenging and has rarely been attempted. Here, we set up a unique experimental infrastructure, in which we continuously heated the whole plant–soil system, the entire gas exchange system and the tubing connected to the isotope laser spectrometers (Fig. S2), to avoid condensation. Consistent with the theory that saturation vapour pressure in the air increases exponentially with increasing temperature (Goff & Gratch, 1946), the measured RH in the cuvette increased accordingly with increasing T_{cuv} to maintain LAVPD of *c*. 0.8 kPa between 5 and 40°C (Fig. 1). T_{leaf} closely followed and was only slightly higher than T_{cuv} (Fig. S3). This demonstrates the utility of our set-up as an effective tool to study unknown plant physiological responses to extreme temperature at constant LAVPD conditions.

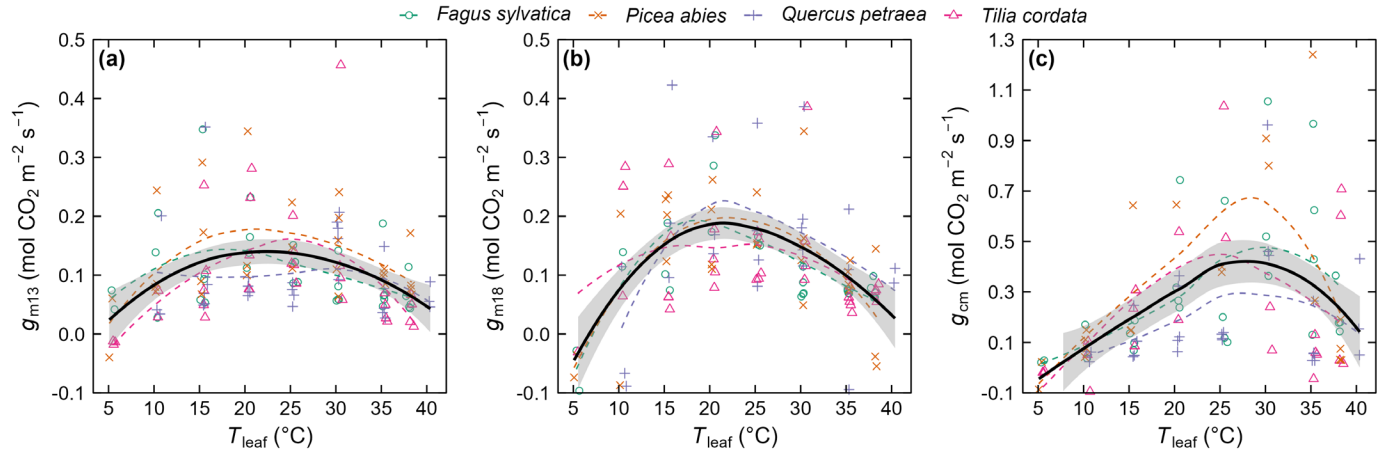

Fig. 4 Leaf temperature (T_{leaf}) response of mesophyll conductance (g_m) for CO_2 in four temperate tree species. Mesophyll conductance to CO_2 estimated from ^{13}C measurements (g_{m13}) represents the total mesophyll conductance (a); mesophyll conductance to CO_2 estimated from ^{18}O measurements (g_{m18}) represents the cell wall and plasma membrane conductance (b); and chloroplast membrane conductance to CO_2 (g_{cm}) is calculated as the difference between g_{m13} and g_{m18} (c). Each dashed line represents the smoothed trend for one species. The solid line and the grey band represent the smoothed trend averaged across all species and its SE, respectively. Different symbols and colours indicate different tree species ($n = 5$, per step of c. 5°C).

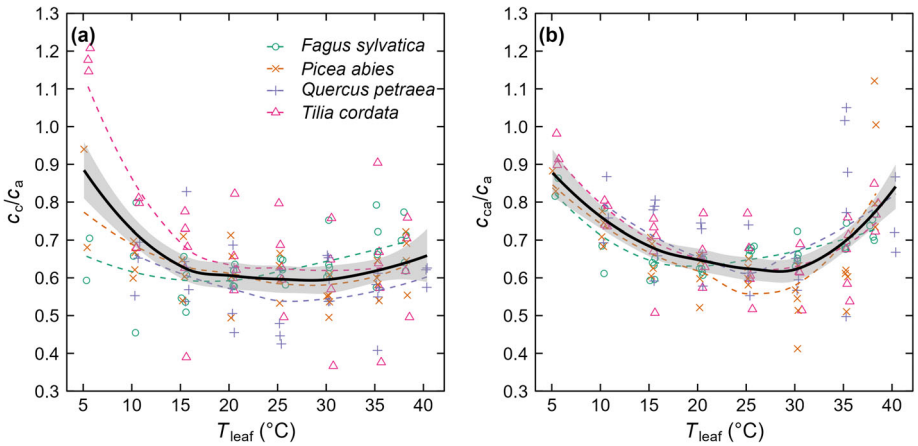

Fig. 5 Leaf temperature (T_{leaf}) responses of the ratio of chloroplastic to ambient CO_2 mole fraction (c_c/c_a; a) and the ratio of CO_2 mole fraction at the sites of carbonic anhydrase activity to ambient CO_2 mole fraction (c_{ca}/c_a; b) in four temperate tree species. c_c and c_{ca} represent the CO_2 mole fraction inside the chloroplast stroma and at the chloroplast surface, respectively. Each dashed line represents the smoothed trend for one species; the solid line and the grey band represent the smoothed trend averaged across all species and its SE, respectively. Different symbols and colours indicate different tree species ($n = 5$, per step of c. 5°C).

Decoupling of photosynthesis and stomatal conductance under the perspective of diffusional CO_2 supply

The reduction in A_n at higher temperatures (> 30°C; Fig. 2a) was not associated with stomatal closure and consequently declining c_i, as the opposite was shown by the patterns of c_i/c_a and g_s (Fig. 2c,d). On the contrary, although $\Delta^{13}C_{obs}$ followed the same trend as c_i/c_a at lower temperatures, this was not the case at higher temperatures (Figs 2d, 3a). Our findings are inconsistent with the simplified $\Delta^{13}C$ model, which describes a linear, positive correlation between $\Delta^{13}C$ and c_i/c_a (Farquhar *et al.*, 1982). This suggests that above the optimum temperature for photosynthesis, factors other than g_s and c_i become increasingly important in determining A_n and $\Delta^{13}C_{obs}$. Intuitively, one of these factors is linked to g_m.

Previous studies on the response of g_m to T_{leaf} have usually indicated that g_m increases with increasing T_{leaf} at low temperatures, whereas the results are mixed at high temperatures (Warren & Dreyer, 2006; Yamori *et al.*, 2006; Evans & von Caemmerer, 2013; Walker *et al.*, 2013; von Caemmerer & Evans, 2015; Shrestha *et al.*, 2019). For the first time, we show that, at a constant LAVPD, g_m and its components generally decrease at high temperatures (Fig. 4). A reduction in g_m is widely thought to reduce CO_2 diffusion from intercellular airspace within a leaf to the sites of carboxylation within chloroplasts, therefore restricting the CO_2 availability at the sites where Rubisco is located in the chloroplast stroma. One could reasonably ask whether this likely led to the observed decreasing A_n. However, our calculations of c_c do not support this explanation; c_c instead remained relatively constant, even slightly increased, at the highest T_{leaf} (Fig. 5a). It therefore appears that A_n and g_m declined in a coordinated fashion, rather than the reduction in A_n being caused by decreasing g_m.

When we extended the calculations further to estimate the CO_2 concentration at the chloroplast surface (i.e. c_{ca}, estimated from $\Delta^{18}O$), the pattern with T_{leaf} was similar in shape to that for c_i (Figs 2d, 5b). This pattern contrasts with that of the CO_2 concentration inside the chloroplast stroma (i.e. c_c, estimated

from $\Delta^{13}C$; Fig. 5a) at temperatures above *c.* 30°C. These observations together suggest active control of plasma and chloroplast membranes to regulate the CO_2 concentration at the sites of Rubisco, possibly through aquaporins that also facilitate CO_2 diffusion (Chen *et al.*, 2023). Having a relatively constant CO_2 supply inside the chloroplast stroma can be beneficial for enzyme functioning at high temperatures, with the result that A_n was not completely supressed at 40°C but was maintained at a level similar to that at *c.* 15–20°C (Fig. 2a).

Based on the evidence mentioned above, we suggest that the cause for the decreasing A_n at high temperatures cannot be a restricted supply of CO_2 to Rubisco through reduced g_m. Instead, we conclude that the reduction in A_n is partially related to Rubisco deactivation, because of the heat sensitivity of Rubisco activase, and therefore a loss of active Rubisco catalytic sites at high temperatures (Crafts-Brandner & Salvucci, 2000; June *et al.*, 2004; Mathur *et al.*, 2014; Scafaro *et al.*, 2023). Another contributing factor is a reduction in the chloroplast electron transport rate as T_{leaf} rises, related to the heat sensitivity of thylakoid membranes and their constituents (Crafts-Brandner & Salvucci, 2000; June *et al.*, 2004; Mathur *et al.*, 2014; Scafaro *et al.*, 2023). Moreover, based on the findings of Scafaro *et al.* (2023), the decline in A_n at high temperatures cannot be caused by increased CO_2 loss from photorespiration and respiration.

Decoupling of photosynthesis and stomatal conductance under the perspective of evaporative cooling

We found that water loss, indicated by E and g_s, did not follow the decrease in A_n at high temperatures, but rather increased continuously up to the maximum T_{cuv} value of 40°C in our experiment. These results clearly show that leaves can increase transpiration by opening stomata without a change in the atmospheric humidity driving force (i.e. LAVPD). This finding aligns well with the study of Urban *et al.* (2017), who found increased g_s with increasing T_{leaf} between 30 and 40°C at a LAVPD of 1 kPa for *Populus deltoides* × *nigra* and *Pinus taeda*. The progressively decreasing $\delta^{18}O_i$ (Fig. 3b) as T_{leaf} increased (corresponding to increasing RH, Fig. 1) in our study is consistent with a negative relationship between leaf water ^{18}O enrichment and RH predicted by the Craig–Gordon equation (Craig & Gordon, 1965; Farquhar *et al.*, 2007). This shows coherence between our gas exchange and isotopic measurements.

The increase in E at high temperatures is partly related to the decline in the viscosity of H_2O with increasing temperature, which improved the water supply to the evaporative sites at the surfaces within the leaf intercellular cavities (Fredeen & Sage, 1999; Cochard *et al.*, 2000). As shown by Roderick & Berry (2001), the fluidity (inverse of viscosity) of water is doubled over the temperature range of 5 to 40°C (Fig. S5). By contrast, any reductions in membrane fluidity and permeability in the leaf as indicated by the decline in g_m (Fig. 4) apparently had little impact on water transport through the leaf mesophyll, which presumably occurs at least partly through aquaporins (Uehlein *et al.*, 2008). We acknowledge that our experimental conditions may have facilitated improved water transport, as the whole plant–soil system, and therefore the water within it, was heated along with the leaves in the gas exchange cuvette. In this regard, however, our experimental set-up is quite relevant for natural ecosystems. The increase in E can be additionally explained by stimulated stomatal opening at high temperatures from a biochemical perspective. Incubation experiments using isolated leaf tissues have shown that heat promotes stomatal opening, by stimulating phototropins and H^+-ATPase activities, as well as by deactivating the production of reactive oxygen species (ROS; Feller, 2006; Devireddy *et al.*, 2020; Driesen *et al.*, 2020; Kostaki *et al.*, 2020). As the molecular machinery needed to perceive temperature changes is located in guard cells independent of the mesophyll layer (Kostaki *et al.*, 2020), direct regulation of g_s through the sensing of temperature by guard cell signals is possible. The positive response of cuticle conductance to increasing temperature could also contribute significantly to E at high temperatures (Eamus *et al.*, 2008; Duursma *et al.*, 2019; Aparecido *et al.*, 2020), although the direct temperature effect, particularly under low LAVPD conditions, on cuticle conductance is still not clear (Slot *et al.*, 2021).

Stomata may open at high temperatures to increase E and thereby cool the leaves (Crawford *et al.*, 2012). Although we did not investigate the direct cooling effect of E on T_{leaf} with rising temperature, that is by comparing T_{leaf} of normal leaves and of leaves with blocked stomates (Clum, 1926; Lin *et al.*, 2017), we observed a minor cooling effect of E on T_{leaf} when using T_{cuv} as a reference (i.e. $T_{leaf} - T_{cuv}$; Fig. S3b). This small cooling effect is consistent with a rather low E (maximum rate *c.* 2 mmol H_2O m^{-2} s^{-1}; Fig. 2b), because of the humid conditions inside the leaf cuvette. Moreover, air within the leaf cuvette was strongly circulated with a fan, which minimized the boundary layer resistance for heat transport and maximized convective heat exchange between the leaf and the air; therefore, it reduced the importance of the cooling effect from E. Another explanation is that the temperature difference between the leaf water for transpiration and the leaf surface was small, given that the entire plant–soil system was heated. Consequently, H_2O molecules have not required much additional energy for transpiration, resulting in reduced energy loss from the leaf surface and, therefore, a diminished cooling effect. In addition, the lack of variation in $T_{leaf} - T_{cuv}$ in *P. abies* (Fig. S3b) can be explained by the technical difficulty of using the leaf thermocouple to measure T_{leaf} for needles, which have a 3D structure, rather than a plane, in contact with the thermocouple (Still *et al.*, 2019). We conclude that the evaporative cooling maintained T_{leaf} at values only slightly higher than T_{cuv} and prevented overheating at high temperatures in our experiments (Fig. S3a), which contributed to the moderate A_n at 40°C (Fig. 2a).

Implications for natural conditions and modelling

At ecosystem and regional scales, increased transpiration from trees can lead to higher latent heat flux and cloud cover, resulting in decreased regional surface temperatures. This, in turn, has a positive effect on the ability of trees to tolerate heat extremes. For

both well-watered plants in a climate chamber and vegetation in the field, enhanced transpirational cooling occurs at the expense of fast consumption of soil water and, as shown in this study, a reduction in WUE (Fig. S4). We are confident that, in our case, the water supply for E was sustained even in the high T_{cuv} range because the plants were well watered throughout the experiment (Schönbeck *et al.*, 2022). In a whole-tree chamber study at the canopy scale (but not under constant VPD conditions), Drake *et al.* (2018) reported A_n–g_s decoupling in *Eucalyptus parramattensis* trees during an artificial heatwave of 4 d with temperatures > 43°C. In their study, drought stress was imposed by withholding irrigation for the month before the heatwave. However, the deep-rooted *Eucalyptus* trees had access to deep soil water and groundwater and thus sustained a functional hydraulic system that allowed enhanced E during the heatwave. Similarly, Krich *et al.* (2022) investigated 13 Australian woody ecosystems and observed a decoupling of A_n and E at high temperatures in four Mediterranean woodlands, which were assumed to have access to some water reserves even after long rainfall deficits. These studies suggest that access to sufficient water reserves during heat waves is a prerequisite for the A_n–g_s decoupling. Nevertheless, a recent study showed that the A_n and g_s decoupling occurred regardless of plant water access; the increase in g_s was even more pronounced for droughted plants than well-watered plants under hot conditions (Marchin *et al.*, 2023). More studies are needed to gain a comprehensive understanding of how the decoupling behaves with changes in soil water supply.

To our knowledge, although efforts have been made to improve the predictions of stomatal models by considering the plant and soil water status, including the effects of abscisic acid synthesis and turgor regulation of guard cells, none of the current models incorporate the mechanism of A_n–g_s decoupling at high temperatures (Damour *et al.*, 2010). This is also true for major climate models which estimate global carbon and water fluxes (Berry *et al.*, 2010). This may lead to underestimations of the capacity of plants to cope with heat extremes and cause biased predictions of evapotranspiration under extreme hot conditions. Incorporating the direct responses of leaf gas exchange and g_m and its components to extreme temperature can help improve the predictions of stomatal and climate models.

Acknowledgements

We acknowledge technical support from the WSL Stable Isotope Research Centre, specifically assistance provided by Manuela Oettli. We acknowledge contributions from Herbert Kurmann, Max Hälg and Walter Godli in setting up the infrastructure. The study was supported by the Swiss National Science Foundation (PZ00P2_179978 and IZCOZ0_205492 granted to MML, as well as 206021_189724 granted to AG and MS) and by WSL Birmensdorf (innovative research grant PPF2020 granted to MML and a visiting fellowship granted to LAC).

Competing interests

None declared.

Author contributions

RTWS, LAC, MML and HD conceived the study. MML supervised the project. HD and RTWS set up the instrumentation and carried out the experimental work. HD and LAC processed the experimental data and performed the analysis. HD wrote the manuscript. LAC, MS, AG, RTWS and MML critically contributed to the manuscript.

ORCID

Lucas A. Cernusak https://orcid.org/0000-0002-7575-5526
Haoyu Diao https://orcid.org/0000-0002-8404-1998
Arthur Gessler https://orcid.org/0000-0002-1910-9589
Marco M. Lehmann https://orcid.org/0000-0003-2962-3351
Matthias Saurer https://orcid.org/0000-0002-3954-3534
Rolf T. W. Siegwolf https://orcid.org/0000-0002-0249-0651

Data availability

All data used in this study are available in the Supporting Information.

References

Adnew GA, Pons TL, Koren G, Peters W, Röckmann T. 2020. Leaf-scale quantification of the effect of photosynthetic gas exchange on $\Delta^{17}O$ of atmospheric CO_2. *Biogeosciences* **17**: 3903–3922.

Ameye M, Wertin TM, Bauweraerts I, McGuire MA, Teskey RO, Steppe K. 2012. The effect of induced heat waves on *Pinus taeda* and *Quercus rubra* seedlings in ambient and elevated CO_2 atmospheres. *New Phytologist* **196**: 448–461.

Aparecido LMT, Woo S, Suazo C, Hultine KR, Blonder B. 2020. High water use in desert plants exposed to extreme heat. *Ecology Letters* **23**: 1189–1200.

Aphalo PJ, Jarvis PG. 1991. Do stomata respond to relative humidity? *Plant, Cell & Environment* **14**: 127–132.

Ball JT, Woodrow IE, Berry JA. 1987. A model predicting stomatal conductance and its contribution to the control of photosynthesis under different environmental conditions. In: Biggins J, ed. *Progress in photosynthesis research: Volume 4 Proceedings of the VIIth international congress on photosynthesis Providence, Rhode Island, USA, August 10–15, 1986*. Dordrecht, the Netherlands: Springer Netherlands, 221–224.

Barbour MM. 2017. Understanding regulation of leaf internal carbon and water transport using online stable isotope techniques. *New Phytologist* **213**: 83–88.

Barbour MM, Evans JR, Simonin KA, von Caemmerer S. 2016. Online CO_2 and H_2O oxygen isotope fractionation allows estimation of mesophyll conductance in C_4 plants, and reveals that mesophyll conductance decreases as leaves age in both C_4 and C_3 plants. *New Phytologist* **210**: 875–889.

Berry JA, Beerling DJ, Franks PJ. 2010. Stomata: key players in the earth system, past and present. *Current Opinion in Plant Biology* **13**: 232–239.

Busch FA, Holloway-Phillips M, Stuart-Williams H, Farquhar GD. 2020. Revisiting carbon isotope discrimination in C_3 plants shows respiration rules when photosynthesis is low. *Nature Plants* **6**: 245–258.

von Caemmerer S, Evans JR. 2015. Temperature responses of mesophyll conductance differ greatly between species. *Plant, Cell & Environment* **38**: 629–637.

von Caemmerer S, Farquhar GD. 1981. Some relationships between the biochemistry of photosynthesis and the gas exchange of leaves. *Planta* **153**: 376–387.

Cernusak LA, Barbour MM, Arndt SK, Cheesman AW, English NB, Feild TS, Helliker BR, Holloway-Phillips MM, Holtum JAM, Kahmen A *et al.* 2016.

Stable isotopes in leaf water of terrestrial plants. *Plant, Cell & Environment* **39**: 1087–1102.

Cernusak LA, Farquhar GD, Wong SC, Stuart-Williams H. 2004. Measurement and interpretation of the oxygen isotope composition of carbon dioxide respired by leaves in the dark. *Plant Physiology* **136**: 3350–3363.

Chen J, Yue K, Shen L, Zheng C, Zhu Y, Han K, Kai L. 2023. Aquaporins and CO_2 diffusion across biological membrane. *Frontiers in Physiology* **14**: 1205290.

Clum HH. 1926. The effect of transpiration and environmental factors on leaf temperatures I. Transpiration. *American Journal of Botany* **13**: 194–216.

Cochard H, Martin R, Gross P, Bogeat-Triboulot MB. 2000. Temperature effects on hydraulic conductance and water relations of *Quercus robur* L. *Journal of Experimental Botany* **51**: 1255–1259.

Crafts-Brandner SJ, Salvucci ME. 2000. Rubisco activase constrains the photosynthetic potential of leaves at high temperature and CO_2. *Proceedings of the National Academy of Sciences, USA* **97**: 13430–13435.

Craig H, Gordon LI. 1965. Deuterium and oxygen-18 variations in the ocean and the marine atmosphere. In: Tongiorgi E, ed. *Proceedings of a conference on stable isotopes in oceanographic studies and palaeotemperatures*. Pisa, Italy: Lischi and Figli, 9–130.

Crawford AJ, McLachlan DH, Hetherington AM, Franklin KA. 2012. High temperature exposure increases plant cooling capacity. *Current Biology* **22**: R396–R397.

Crous KY, Uddling J, De Kauwe MG. 2022. Temperature responses of photosynthesis and respiration in evergreen trees from boreal to tropical latitudes. *New Phytologist* **234**: 353–374.

Damour G, Simonneau T, Cochard H, Urban L. 2010. An overview of models of stomatal conductance at the leaf level. *Plant, Cell & Environment* **33**: 1419–1438.

De Kauwe MG, Medlyn BE, Pitman AJ, Drake JE, Ukkola A, Griebel A, Pendall E, Prober S, Roderick M. 2019. Examining the evidence for decoupling between photosynthesis and transpiration during heat extremes. *Biogeosciences* **16**: 903–916.

Devireddy AR, Arbogast J, Mittler R. 2020. Coordinated and rapid whole-plant systemic stomatal responses. *New Phytologist* **225**: 21–25.

Drake JE, Tjoelker MG, Vårhammar A, Medlyn Belinda E, Reich PB, Leigh A, Pfautsch S, Blackman CJ, López R, Aspinwall MJ *et al.* 2018. Trees tolerate an extreme heatwave via sustained transpirational cooling and increased leaf thermal tolerance. *Global Change Biology* **24**: 2390–2402.

Driesen E, Van den Ende W, De Proft M, Saeys W. 2020. Influence of environmental factors light, CO_2, temperature, and relative humidity on stomatal opening and development: A review. *Agronomy* **10**: 1975.

Duursma RA, Barton CVM, Lin Y-S, Medlyn BE, Eamus D, Tissue DT, Ellsworth DS, McMurtrie RE. 2014. The peaked response of transpiration rate to vapour pressure deficit in field conditions can be explained by the temperature optimum of photosynthesis. *Agricultural and Forest Meteorology* **189–190**: 2–10.

Duursma RA, Blackman CJ, Lopéz R, Martin-StPaul NK, Cochard H, Medlyn BE. 2019. On the minimum leaf conductance: its role in models of plant water use, and ecological and environmental controls. *New Phytologist* **221**: 693–705.

Eamus D, Taylor DT, Macinnis-NG CMO, Shanahan S, de Silva L. 2008. Comparing model predictions and experimental data for the response of stomatal conductance and guard cell turgor to manipulations of cuticular conductance, leaf-to-air vapour pressure difference and temperature: feedback mechanisms are able to account for all observations. *Plant, Cell & Environment* **31**: 269–277.

Eludoyin OM, Adelekan IO, Webster R, Eludoyin AO. 2014. Air temperature, relative humidity, climate regionalization and thermal comfort of Nigeria. *International Journal of Climatology* **34**: 2000–2018.

Evans J, Sharkey T, Berry J, Farquhar G. 1986. Carbon isotope discrimination measured concurrently with gas exchange to investigate CO_2 diffusion in leaves of higher plants. *Functional Plant Biology* **13**: 281–292.

Evans JR, von Caemmerer S. 2013. Temperature response of carbon isotope discrimination and mesophyll conductance in tobacco. *Plant, Cell & Environment* **36**: 745–756.

Farquhar G, Wong S. 1984. An empirical model of stomatal conductance. *Functional Plant Biology* **11**: 191–210.

Farquhar GD, Cernusak LA. 2012. Ternary effects on the gas exchange of isotopologues of carbon dioxide. *Plant, Cell & Environment* **35**: 1221–1231.

Farquhar GD, Cernusak LA, Barnes B. 2007. Heavy water fractionation during transpiration. *Plant Physiology* **143**: 11–18.

Farquhar GD, O'Leary MH, Berry JA. 1982. On the relationship between carbon isotope discrimination and the intercellular carbon dioxide concentration in leaves. *Functional Plant Biology* **9**: 121–137.

Feller U. 2006. Stomatal opening at elevated temperature: an underestimated regulatory mechanism. *General and Applied Plant Physiology* **32**: 19–31.

Feng X, Liu R, Li C, Zhang H, Slot M. 2023. Contrasting responses of two C4 desert shrubs to drought but consistent decoupling of photosynthesis and stomatal conductance at high temperature. *Environmental and Experimental Botany* **209**: 105295.

Flexas J, Diaz-Espejo A. 2015. Interspecific differences in temperature response of mesophyll conductance: food for thought on its origin and regulation. *Plant, Cell & Environment* **38**: 625–628.

Frank D, Reichstein M, Bahn M, Thonicke K, Frank D, Mahecha MD, Smith P, van der Velde M, Vicca S, Babst F *et al.* 2015. Effects of climate extremes on the terrestrial carbon cycle: concepts, processes and potential future impacts. *Global Change Biology* **21**: 2861–2880.

Fredeen AL, Sage RF. 1999. Temperature and humidity effects on branchlet gas-exchange in white spruce: an explanation for the increase in transpiration with branchlet temperature. *Trees* **14**: 161–168.

Gillon JS, Yakir D. 2000. Internal conductance to CO_2 diffusion and $C^{18}OO$ discrimination in C_3 leaves. *Plant Physiology* **123**: 201–214.

Goff JA, Gratch S. 1946. Low-pressure properties of water from −160 to 212F. *Transactions of the American Society of Heating and Ventilating Engineers* **52**: 95–122.

Grossiord C, Buckley TN, Cernusak LA, Novick KA, Poulter B, Siegwolf RTW, Sperry JS, McDowell NG. 2020. Plant responses to rising vapor pressure deficit. *New Phytologist* **226**: 1550–1566.

Hall AE, Camacho-B SE, Kaufmann MR. 1975. Regulation of water loss by citrus leaves. *Physiologia Plantarum* **33**: 62–65.

Hall AE, Kaufmann MR. 1975. Stomatal response to environment with *Sesamum indicum L. Plant Physiology* **55**: 455–459.

Hamerlynck E, Knapp AK. 1996. Photosynthetic and stomatal responses to high temperature and light in two oaks at the western limit of their range. *Tree Physiology* **16**: 557–565.

Hastie T. 2023. *GAM: generalized additive models*, v1.22-3. [WWW document] URL https://cran.r-project.org/web/packages/gam/index.html [accessed 10 January 2024].

Holloway-Phillips M, Cernusak LA, Stuart-Williams H, Ubierna N, Farquhar GD. 2019. Two-source $\delta^{18}O$ method to validate the $CO^{18}O$-photosynthetic discrimination model: Implications for mesophyll conductance. *Plant Physiology* **181**: 1175–1190.

IPCC. 2021. In: Masson-Delmotte V, Zhai P, Pirani A, Connors SL, Péan C, Berger S, Caud N, Chen Y, Goldfarb L, Gomis MI *et al.*, eds. *Climate Change 2021: the physical science basis. Contribution of working group I to the sixth assessment report of the Intergovernmental Panel on Climate Change*. Cambridge, UK and New York, NY, USA: Cambridge University Press.

June T, Evans JR, Farquhar GD. 2004. A simple new equation for the reversible temperature dependence of photosynthetic electron transport: a study on soybean leaf. *Functional Plant Biology* **31**: 275–283.

Khan PI, Ratnam DV, Prasad P, Basha G, Jiang JH, Shaik R, Ratnam MV, Kishore P. 2022. Observed climatology and trend in relative humidity, CAPE, and CIN over India. *Atmosphere* **13**: 361.

Kodama N, Cousins A, Tu KP, Barbour MM. 2011. Spatial variation in photosynthetic CO_2 carbon and oxygen isotope discrimination along leaves of the monocot triticale (*Triticum* × *Secale*) relates to mesophyll conductance and the Péclet effect. *Plant, Cell & Environment* **34**: 1548–1562.

Kostaki K-I, Coupel-Ledru A, Bonnell VC, Gustavsson M, Sun P, McLaughlin FJ, Fraser DP, McLachlan DH, Hetherington AM, Dodd AN *et al.* 2020. Guard cells integrate light and temperature signals to control stomatal aperture. *Plant Physiology* **182**: 1404–1419.

Krich C, Mahecha MD, Migliavacca M, De Kauwe MG, Griebel A, Runge J, Miralles DG. 2022. Decoupling between ecosystem photosynthesis and

transpiration: a last resort against overheating. *Environmental Research Letters* **17**: 44013.

Kupper P, Sellin A, Tenhunen J, Schmidt M, Rahi M. 2006. Effects of branch position on water relations and gas exchange of European larch trees in an alpine community. *Trees* **20**: 265–272.

Kuznetsova A, Brockhoff PB, Christensen RHB. 2017. LMERTEST package: tests in linear mixed effects models. *Journal of Statistical Software* **82**: 1–26.

Lawson T, von Caemmerer S, Baroli I. 2011. Photosynthesis and stomatal behaviour. In: Lüttge UE, Beyschlag W, Büdel B, Francis D, eds. *Progress in botany 72*. Berlin, Heidelberg, Germany: Springer Berlin Heidelberg, 265–304.

Leuning R, Kelliher FM, De Pury DGG, Sschulze E-D. 1995. Leaf nitrogen, photosynthesis, conductance and transpiration: scaling from leaves to canopies. *Plant, Cell & Environment* **18**: 1183–1200.

Lin H, Chen Y, Zhang H, Fu P, Fan Z. 2017. Stronger cooling effects of transpiration and leaf physical traits of plants from a hot dry habitat than from a hot wet habitat. *Functional Ecology* **31**: 2202–2211.

Marchin RM, Medlyn BE, Tjoelker MG, Ellsworth DS. 2023. Decoupling between stomatal conductance and photosynthesis occurs under extreme heat in broadleaf tree species regardless of water access. *Global Change Biology* **29**: 6319–6335.

Mathur S, Agrawal D, Jajoo A. 2014. Photosynthesis: response to high temperature stress. *Journal of Photochemistry and Photobiology B: Biology* **137**: 116–126.

McDowell NG, Sapes G, Pivovaroff A, Adams HD, Allen CD, Anderegg WRL, Arend M, Breshears DD, Brodribb T, Choat B *et al.* 2022. Mechanisms of woody-plant mortality under rising drought, CO_2 and vapour pressure deficit. *Nature Reviews Earth & Environment* **3**: 294–308.

Mook WG. 2000. *Environmental isotopes in the hydrological cycle: principles and applications, Vol. I: Introduction; theory, methods, review*. Paris, France: UNESCO.

Mott KA, Peak D. 2010. Stomatal responses to humidity and temperature in darkness. *Plant, Cell & Environment* **33**: 1084–1090.

Novick KA, Ficklin DL, Stoy PC, Williams CA, Bohrer G, Oishi AC, Papuga SA, Blanken PD, Noormets A, Sulman BN *et al.* 2016. The increasing importance of atmospheric demand for ecosystem water and carbon fluxes. *Nature Climate Change* **6**: 1023–1027.

Osonubi O, Davies WJ. 1980. The influence of water stress on the photosynthetic performance and stomatal behaviour of tree seedlings subjected to variation in temperature and irradiance. *Oecologia* **45**: 3–10.

Perkins SE, Alexander LV, Nairn JR. 2012. Increasing frequency, intensity and duration of observed global heatwaves and warm spells. *Geophysical Research Letters* **39**: L20714.

R Core Team. 2023. *R: a language and environment for statistical computing*. Vienna, Austria: R Foundation for Statistical Computing.

Roderick ML, Berry SL. 2001. Linking wood density with tree growth and environment: a theoretical analysis based on the motion of water. *New Phytologist* **149**: 473–485.

Scafaro AP, Posch BC, Evans JR, Farquhar GD, Atkin OK. 2023. Rubisco deactivation and chloroplast electron transport rates co-limit photosynthesis above optimal leaf temperature in terrestrial plants. *Nature Communications* **14**: 2820.

Schönbeck LC, Schuler P, Lehmann MM, Mas E, Mekarni L, Pivovaroff AL, Turberg P, Grossiord C. 2022. Increasing temperature and vapour pressure deficit lead to hydraulic damages in the absence of soil drought. *Plant, Cell & Environment* **45**: 3275–3289.

Schulze ED, Lange OL, Kappen L, Buschbom U, Evenari M. 1973. Stomatal responses to changes in temperature at increasing water stress. *Planta* **110**: 29–42.

Seneviratne SI, Donat MG, Mueller B, Alexander LV. 2014. No pause in the increase of hot temperature extremes. *Nature Climate Change* **4**: 161–163.

Shrestha A, Song X, Barbour MM. 2019. The temperature response of mesophyll conductance, and its component conductances, varies between species and genotypes. *Photosynthesis Research* **141**: 65–82.

Siegwolf RTW, Lehmann MM, Goldsmith GR, Churakova OV, Mirande-Ney C, Timoveeva G, Weigt RB, Saurer M. 2023. Updating the dual C and O isotope—gas-exchange model: a concept to understand plant responses to the environment and its implications for tree rings. *Plant, Cell & Environment* **46**: 2606–2627.

Singh P, Kumar V, Thomas T, Arora M. 2008. Changes in rainfall and relative humidity in river basins in northwest and central India. *Hydrological Processes* **22**: 2982–2992.

Slot M, Nardwattanawong T, Hernández GG, Bueno A, Riederer M, Winter K. 2021. Large differences in leaf cuticle conductance and its temperature response among 24 tropical tree species from across a rainfall gradient. *New Phytologist* **232**: 1618–1631.

Smith MN, Taylor TC, van Haren J, Rosolem R, Restrepo-Coupe N, Adams J, Wu J, de Oliveira RC, da Silva R, de Araujo AC *et al.* 2020. Empirical evidence for resilience of tropical forest photosynthesis in a warmer world. *Nature Plants* **6**: 1225–1230.

Sonawane BV, Cousins AB. 2019. Uncertainties and limitations of using carbon-13 and oxygen-18 leaf isotope exchange to estimate the temperature response of mesophyll CO_2 conductance in C_3 plants. *New Phytologist* **222**: 122–131.

Still CJ, Sibley A, Page G, Meinzer FC, Sevanto S. 2019. When a cuvette is not a canopy: a caution about measuring leaf temperature during gas exchange measurements. *Agricultural and Forest Meteorology* **279**: 107737.

Trotsiuk V, Babst F, Grossiord C, Gessler A, Forrester DI, Buchmann N, Schaub M, Eugster W. 2021. Tree growth in Switzerland is increasingly constrained by rising evaporative demand. *Journal of Ecology* **109**: 2981–2990.

Uehlein N, Otto B, Hanson DT, Fischer M, McDowell N, Kaldenhoff R. 2008. Function of *Nicotiana tabacum* aquaporins as chloroplast gas pores challenges the concept of membrane CO_2 permeability. *Plant Cell* **20**: 648–657.

Urban J, Ingwers MW, McGuire MA, Teskey RO. 2017. Increase in leaf temperature opens stomata and decouples net photosynthesis from stomatal conductance in *Pinus taeda* and *Populus deltoides x nigra*. *Journal of Experimental Botany* **68**: 1757–1767.

Vicente-Serrano SM, Nieto R, Gimeno L, Azorin-Molina C, Drumond A, El Kenawy A, Dominguez-Castro F, Tomas-Burguera M, Peña-Gallardo M. 2018. Recent changes of relative humidity: regional connections with land and ocean processes. *Earth System Dynamics* **9**: 915–937.

Walker B, Ariza LS, Kaines S, Badger MR, Cousins AB. 2013. Temperature response of *in vivo* Rubisco kinetics and mesophyll conductance in *Arabidopsis thaliana*: comparisons to *Nicotiana tabacum*. *Plant, Cell & Environment* **36**: 2108–2119.

Warren C, Dreyer E. 2006. Temperature response of photosynthesis and internal conductance to CO_2: results from two independent approaches. *Journal of Experimental Botany* **57**: 3057–3067.

Wingate L, Seibt U, Moncrieff JB, Jarvis PG, Lloyd J. 2007. Variations in ^{13}C discrimination during CO_2 exchange by *Picea sitchensis* branches in the field. *Plant, Cell & Environment* **30**: 600–616.

Wong SC, Cowan IR, Farquhar GD. 1979. Stomatal conductance correlates with photosynthetic capacity. *Nature* **282**: 424–426.

Yamori W, Noguchi K, Hanba YT, Terashima I. 2006. Effects of internal conductance on the temperature dependence of the photosynthetic rate in spinach leaves from contrasting growth temperatures. *Plant and Cell Physiology* **47**: 1069–1080.

Supporting Information

Additional Supporting Information may be found online in the Supporting Information section at the end of the article.

Fig. S1 Climate envelopes of *Fagus sylvatica*, *Picea abies*, *Quercus petraea* and *Tilia cordata*.

Fig. S2 Schematic of the instrumental set-up.

Fig. S3 Relationships between cuvette temperature (T_{cuv}) and leaf temperature (T_{leaf}) and between transpiration (E) and $T_{leaf} - T_{cuv}$.

Fig. S4 Water-use efficiency responses to leaf temperature (T_{leaf}) for four temperate tree species.

Fig. S5 Normalized fluidity of water responses to temperature.

Methods S1 Supporting information on calculations.

Table S1 Definitions of symbols used repeatedly in the calculations.

Table S2 Dataset analysed in this study.

Please note: Wiley is not responsible for the content or functionality of any Supporting Information supplied by the authors. Any queries (other than missing material) should be directed to the *New Phytologist* Central Office.